NAVIGATION: *Journal of The Institute of Navigation*
Vol. 42, No. 3, Fall 1995
Printed in U.S.A.

Autolanding a 737 Using GPS Integrity Beacons

CLARK E. COHEN, H. STEWART COBB, DAVID G. LAWRENCE, BORIS S. PERVAN, J. DAVID POWELL, and BRADFORD W. PARKINSON

Stanford University, Stanford, California

GERALD J. AUBREY and WILLIAM LOEWE

United Airlines, San Francisco, California

DOUGLAS ORMISTON

Boeing Commercial Airplane Group, Seattle, Washington

B. DAVID MCNALLY and DAVID N. KAUFMANN

NASA Ames Research Center, Mountain View, California

VICTOR WULLSCHLEGER

Federal Aviation Administration Technical Center, Atlantic City, New Jersey

RAYMOND J. SWIDER, JR.

Federal Aviation Administration, Washington, D.C.
Received June 1995
Revised August 1995

ABSTRACT

This paper describes how differential GPS (DGPS) and miniature, low-cost Integrity Beacon pseudolites were used to carry out 110 successful automatic landings of a United Airlines Boeing 737 aircraft. These autopilot-in-the-loop flight tests using GPS Integrity Beacons (low-power, ground-based marker beacon pseudolites placed under the approach path) furnished evidence that GPS can provide the full performance necessary to meet the stringent specifications of Category III. The built-in geometrical redundancy provided by Integrity Beacon ranging is coupled with centimeter-level accuracy to provide the system integrity. This integrity—calculated to be better than one part in a billion probability of missed detection—is achieved independently from ground-based monitors using receiver autonomous integrity monitoring (RAIM).

INTRODUCTION

Landing aircraft in poor visibility imposes the highest known standard of performance for a navigation system. The system must not fail to preserve and protect life and property.

Required to work under harsh weather conditions, a Category III (lowest visibility) landing system must meet a position accuracy requirement (95 percent) at the runway threshold of 2 ft vertically and 13 ft laterally [1]. The integrity requirement for each approach is that the probability of missed detection of failure cannot exceed 0.5×10^{-9} [1]. These specifications have been employed worldwide over the last several decades for the currently operational Instrument Landing System (ILS), and recently for the previously designated follow-on to ILS, the Microwave Landing System (MLS). They have resulted in a perfect safety record. In the United States, the courts have not found any deficiency in ILS over the past 50 years [2]. Debate is currently under way to resolve whether emphasis should be shifted to the touchdown box [3], or whether the vertical performance specifications cited above should be relaxed in any way for GPS, now under consideration as the next landing system standard, and possibly to continue in use for several decades.

This paper presents the results from an October 1994 demonstration of a new Category III landing system based on GPS, carried out on a commercial passenger airliner—a United Airlines Boeing 737. This system uses GPS and Integrity Beacons—compact, low-power, ground-based marker beacon pseudolites (transmitters used as pseudo-GPS satellites)—to satisfy the performance specifications for Category III precision landing of aircraft. A series of 110 autolands was carried out in the 737 (shown in Figure 1) at Crows Landing, California, to test the Integrity Beacon concept. These tests were intended to demonstrate both the accuracy and integrity built into the Integrity Beacon Landing System (IBLS).

Overview of Integrity Beacon Landing System

Stanford University has been developing the Integrity Beacon [4–7] as a means of augmenting GPS to provide the performance required to achieve Category III specifications. Through flight tests [4–7] and analysis, Stanford and the Federal Aviation Administration (FAA) have sought to demonstrate that IBLS provides more than adequate accuracy (by any standard, U.S. or international), and that it has nearly fail-proof integrity (again, by any standard), built upon the centimeter-level precision of carrier phase and the natural redundant cross-checks provided by the system architecture.

IBLS (for which two patent applications have been filed) is illustrated in Figure 2. Integrity Beacons are nominally situated in pairs on either side of the approach path to a runway. The power is set low so that the broadcast signal is measurable only inside the 'bubble' shown in the figure. The bubble radius (determined by the broadcast signal power) is adequate when it is only a few times larger than the nominal altitude of approach. A conventional differential GPS (DGPS) reference station is located at the airport tower. This station broadcasts GPS reference information to all aircraft in the vicinity of the airport—both on the ground and in flight. After being guided to the integrity bubble using traditional DGPS, an aircraft is then capable of tracking enough ranging sources to initialize DGPS to centimeter-level accuracy with a high degree of integrity. The aircraft can then maintain this initialization from bubble exit through touchdown and rollout.

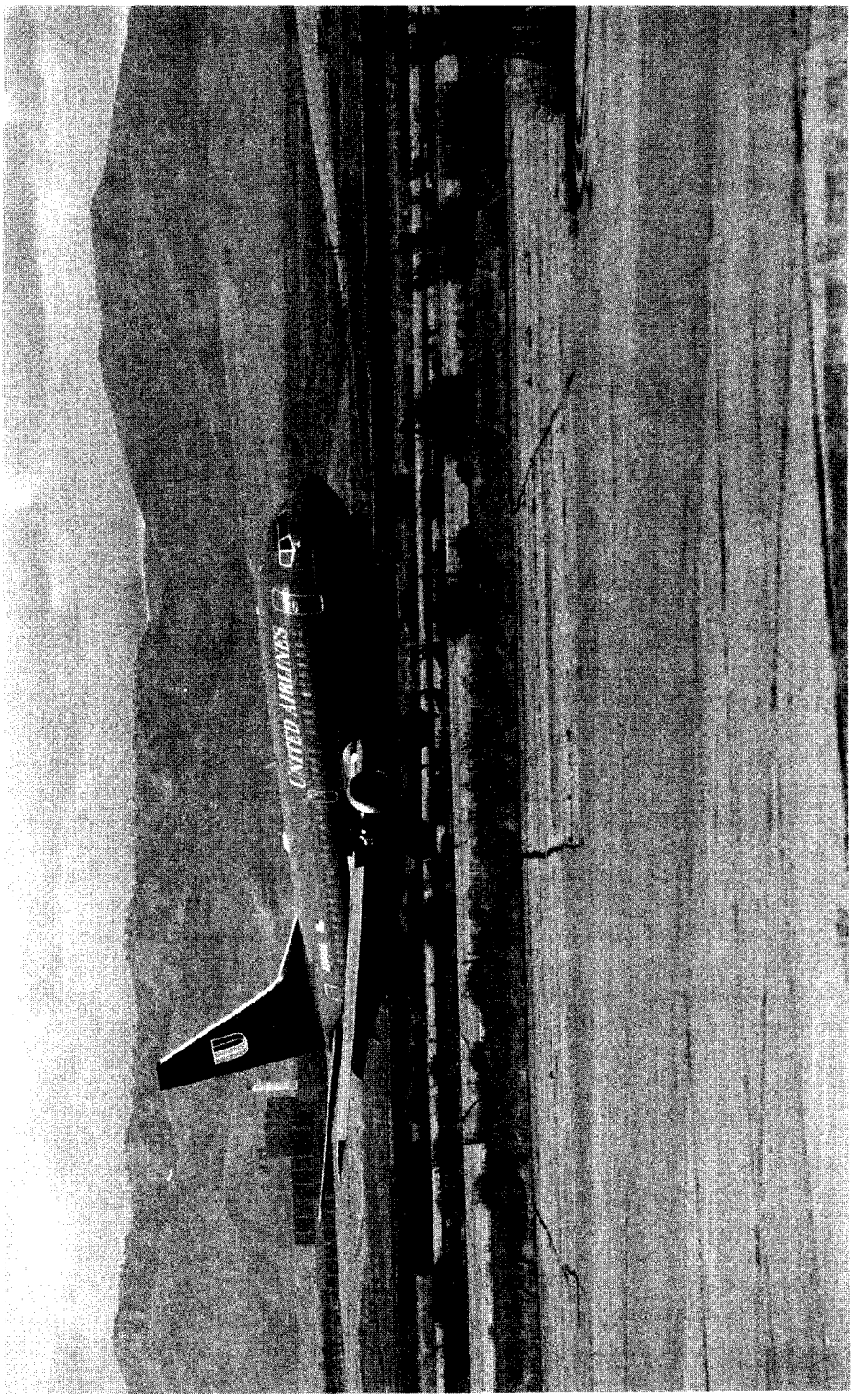

Fig. 1—Boeing 737 Test Aircraft

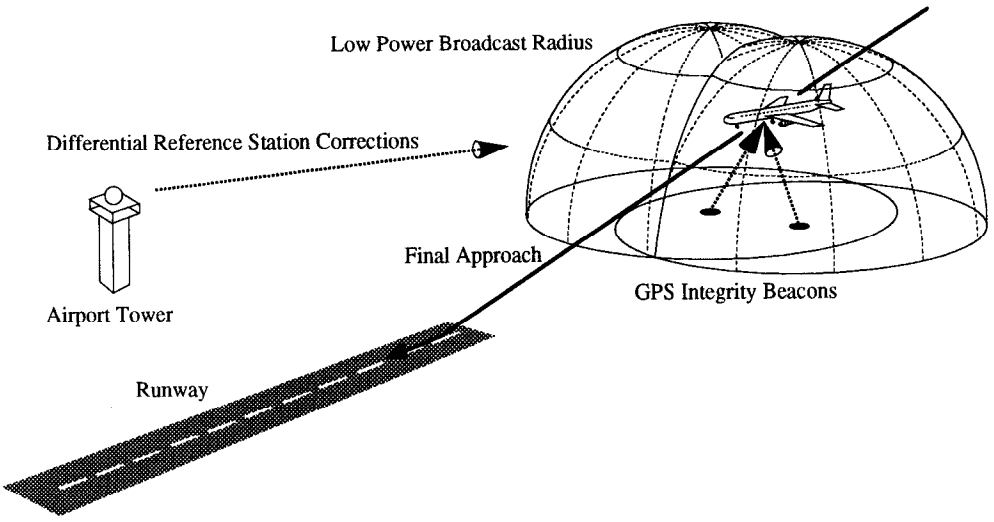

Fig. 2—Integrity Beacon Landing System (IBLS) for Category III Precision Landing

By allowing the aircraft to use the precision of GPS carrier phase reliably, Integrity Beacons provide the aircraft with centimeter-level sensor accuracy. The aircraft receiver can convert this accuracy into a high level of on-board integrity through receiver autonomous integrity monitoring (RAIM). As it flies through the bubble, the aircraft obtains GPS ranging information from every direction—both from the GPS satellites in the sky above and from the Integrity Beacons below, as shown in Figure 3. The six or more effectively independent measurements must agree with one another to within just a few centimeters. If any element of the system is not performing to specification, the inconsistencies among the centimeter-level measurements and the overdetermined solution make the problem clear, and the system issues an integrity alarm. This capability is autonomous, so that the aircraft makes the final integrity decision, not the ground. Related papers discuss these attributes in more detail [8–10]. RAIM provides protection against both known and unknown failure modes. Through analysis and simulation, the intrinsic level of integrity provided by IBLS is derived to be better than one part in a billion [10].

The Integrity Beacon pseudolite fits entirely on a circuit board the size of a credit card. Capable of running on a 9 V battery for over 12 h, it transmits just a few microwatts of power for a standard-size bubble.

IBLS is a spin-off of NASA-sponsored research at Stanford University directed towards a satellite test of Einstein's general theory of relativity. On the spacecraft, called Gravity Probe B, GPS will be used for both precise orbit determination and spacecraft attitude determination. Many of the kinematic positioning techniques pioneered in the attitude system laid groundwork for the landing system. Under FAA sponsorship, the IBLS 'Pathfinder' was developed as a feasibility test bed for Category III precision landing.

AIRBORNE SYSTEM CONFIGURATION

This section describes the airborne component of the system, in terms of both the IBLS sensor itself, and the 737 autopilot and interfaces.

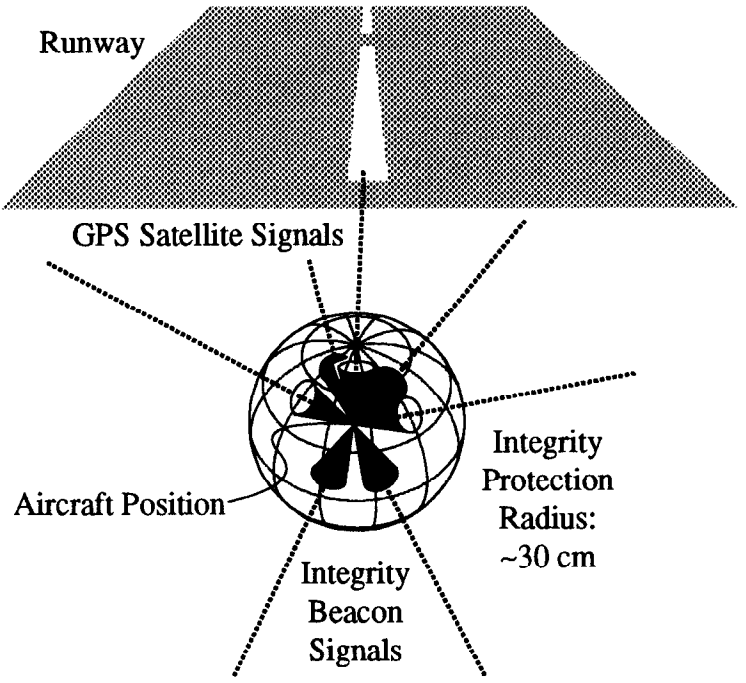

Fig. 3—Integrity Beacon Landing System (IBLS) Offers RAIM for Precision Approach

IBLS Navigation Sensor

The IBLS navigation sensor aboard the aircraft, shown in Figure 4, consists of a GPS receiver, a data link receiver, and a computer to execute the IBLS algorithms. The mathematical framework employed inside the bubble by the computer to resolve the integers is described in Appendix A. After the bubble pass, kinematic positioning, described in Appendix B, guides the aircraft in through touchdown.

During these flight tests, we used a Trimble TANS Quadrex dual-antenna GPS receiver and a ruggedized PC-based computer manufactured by Dolch. The data link was a pair of 9600 baud Dataradio VHF transceivers. Support equipment included an inverter to power the Dolch and the Dataradio from the available 28 V aircraft power bus. We used two GPS antennas: one in the usual place atop the fuselage, and one on the belly of the aircraft to detect the pseudolite signals.

We had originally hoped that the new nine-channel GPS sensor under development would be ready for use for the flight tests. Although the nine-channel system was nearly finished, we decided it would be more prudent to use the older six-channel system that had already undergone significantly more flight testing. The older six-channel system, however, has two central drawbacks: it has circa-1985 code phase measurement quality, and there are only enough channels to track four satellites (and two pseudolites). For these flight tests, the chosen satellite selection algorithm simply tracked the four highest-elevation satellites in the sky, thereby ensuring that the chosen satellites would be well

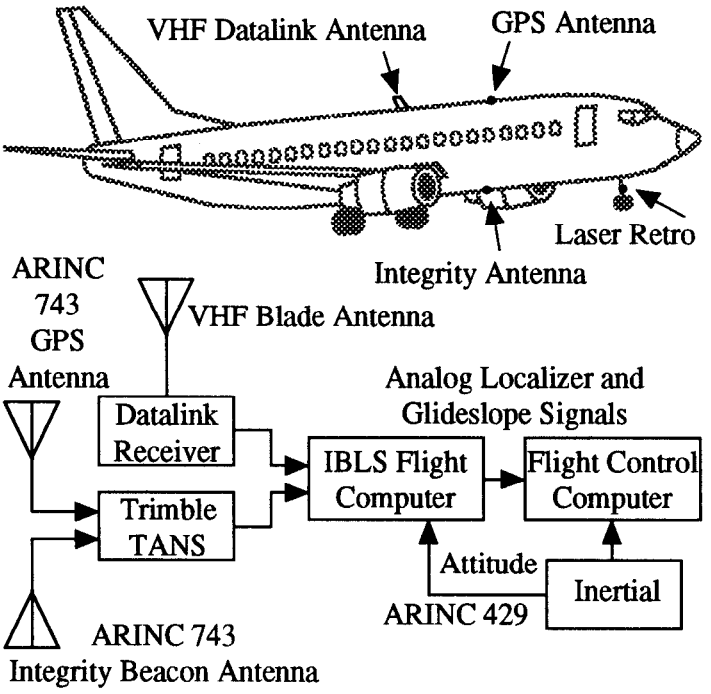

Fig. 4—Airborne Configuration of United 737

inside the antenna field of view. Naturally, although signal strengths of higher-elevation satellites are generally better than those of lower-elevation satellites, this algorithm tends to result in higher position dilution of precision (PDOP) than usual. These experiment-specific (not architecture-specific) GPS sensor characteristics introduced some interesting handicaps for flight testing that were easily overcome by the high precision of carrier phase.

For this experiment, IBLS used an aircraft attitude input from one of the 737 inertial units so that it could carry out the lever-arm correction between its two antennas for higher overall accuracy. The inertial from the 737 provided the attitude data in real time so that the belly-mounted GPS antenna measurements could be projected to the location of the top-mounted antenna.

The autoland flight control system normally accepts localizer and glide slope deviations from the ILS receivers as analog voltages (± 150 mV full scale). We built a pair of PC interface cards to generate localizer and glide slope voltages, with scaling and dynamics to match the ILS receiver specifications. Note that to match the ILS sensor characteristics (which have limited dynamic range and response), the GPS signal had to be delayed and low-pass filtered.

737 Autoland System

The Boeing 737 has a two-autopilot, fail-passive autoland system certified for Category IIIA operations. Since it is certified as a Category IIIA aircraft, it does not provide rollout guidance, and both autopilots disconnect automatically at touchdown. Output from the IBLS system emulated the output from the ILS receivers, while providing the necessary discretes to enable the autoland

system. A special switch was provided for pilot selection of ILS or GPS guidance. When GPS guidance was selected, all autopilot inputs and cockpit displays functioned as if an ILS approach were being executed, though GPS was the guidance source.

The Boeing 737 autoland flight control system (FCS) is fully redundant, with dual systems cross-checking each other at every stage. The system architecture depends on the assumption that inputs come from independent, redundant hardware devices with no undetectable common failure modes. We proposed to 'mislead' the FCS by splitting off the output signal from a single IBLS for use as dual redundant signals to be fed to the two separate flight control computers. This presented a certain safety concern, since the same IBLS hardware was feeding both autopilots. Certain failures in the IBLS brassboard would not be detectable through flight system redundancy. We addressed these potential failures as follows.

The IBLS software is still experimental. Although it has been tested flying under visual flight rules (VFR) conditions with hundreds of approaches both in flight and in ground simulations, it was still in our estimation the most likely element of the system to fail. Therefore, it would make little sense to duplicate the relatively reliable IBLS hardware in the name of redundancy, simply to run a second copy of the same IBLS software. Instead, we decided to duplicate only the IBLS hardware 'downstream' of the software, and to provide it with features to detect the most likely failures, conjectured to be data jumps or system freeze-ups.

Accordingly, we built two analog output boards, each of which simulated the electrical outputs of a single ILS receiver. A hardware failure in one of these boards would be detected by the same FCS algorithms normally used to detect an ILS receiver failure. The relatively long time constants of these outputs provided protection against a sudden hardover software failure (where the output or signal jumps to an extreme value, possibly saturating an input). Furthermore, the boards were provided with watchdog timers that would negate the "ILS Tuned" discrete to the FCS if they were not reset every second by the software. If this discrete is negated during an approach, it causes the autopilot to disconnect immediately, with the usual warnings to the pilot. We thus protected against failures in which the software simply stopped operating.

Prior to flight tests with the GPS system installed, autoland software simulation data provided an assessment of the effect of the GPS-derived pseudo-ILS signals on the autoland system. This in turn provided the capability of performing simulated approach path captures and autolands, comparing the results with ILS approaches. For the numerical simulations, the aircraft was assumed to be of nominal configuration, and flown in both calm air, and winds and turbulence.

Simulated approaches were flown using the signal characteristics expected from the GPS system, including a 5 Hz update rate and signal latency of up to 250 ms. Several cases were also flown with a bias that was removed at 600 ft above ground level (AGL) to simulate the resolving of the ambiguities. Before flight tests, this bias, or error, was expected to be on the order of 2 m using the new nine-channel GPS system. The older six-channel system used for the actual flight tests exhibited somewhat larger jumps at bubble exit,

depending on the specific PDOP and carrier noise. An update rate of 4 Hz was used to drive the autopilot for most of the landings.

In the configuration used for the flight tests, certain failures of the GPS unit could have caused the pseudo-ILS signals to fail hardover, thus saturating the inputs of both autopilots. Simulated hardovers were initiated at various altitudes. For each altitude, two cases were performed: one in which the hardover was allowed to remain indefinitely, and one in which go-around was engaged after 1 s. These simulations were used to analyze the acceptability of the single-channel configuration for the flight tests.

GROUND SYSTEM CONFIGURATION

This section describes the ground-based components of the system, as well as the laser tracking system.

IBLS Ground Station

Figure 5 shows a block diagram of the complete ground system using the Integrity Beacon. The signals from the beacons are fed directly into the differential reference station. The reference station measures the carrier phase of both the Integrity Beacon signals and the GPS satellite signals. Both sets of measurements are transmitted as a group up to the aircraft via the traditional differential data link at 2 Hz. The ground equipment was located underneath the approach path roughly 3.8 km out from the aimpoint. This corresponds to an approximate pseudolite overflight altitude of 600 ft.

NASA Crow's Landing Flight Test Facilities

All test flights were conducted at NASA Ames Research Center's Crows Landing Flight Facility, located approximately 45 mi east of Mountain View, California. The NdYAG laser tracker provides precise aircraft range, azimuth, and elevation, and is used to provide the GPS time-tagged truth reference data

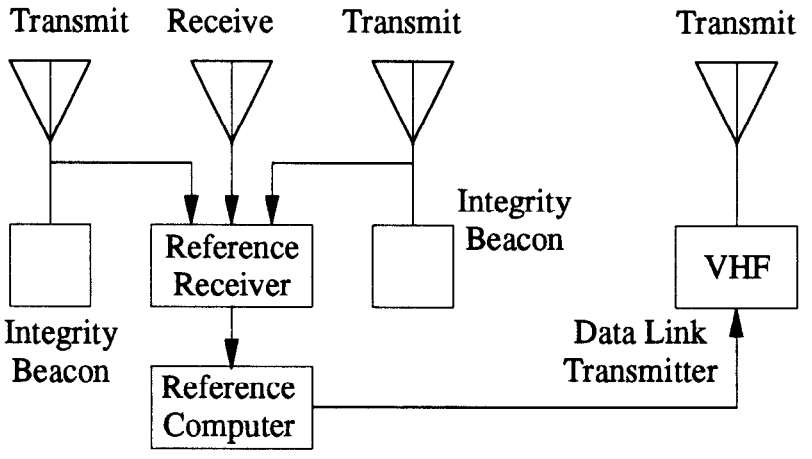

Fig. 5—Integrity Beacon Landing System (IBLS) Ground Equipment

by tracking a laser retroreflector mounted on the test aircraft. The advertised laser tracker range accuracy is nominally ±1 ft (1 σ); azimuth and elevation accuracy are nominally ±0.2 mrad (1 σ). However, experience with the laser tracker during these and other approach and landing flight tests has demonstrated consistently better accuracies.

The laser tracker was calibrated immediately prior to the start of the series of approaches during each flight test. In addition, the laser tracker was checked after each approach by tracking a static laser retroreflector mounted at a survey point located approximately underneath the 100 ft height above the runway threshold point along the 3 deg approach path. In the laser truth reference data postprocessing, 'wild points' from the laser tracker were removed from the azimuth and elevation data, and the remaining data were then smoothed with a zero-phase-shift, low-pass digital filter.

FLIGHT TEST RESULTS

This section presents the flight test results for the 110 autolands of the United 737.

Summary of Flight Test Procedures

The flight test consisted of standard 3 deg flight path straight-in approaches terminating with autolands to Runway 35 at the Crows Landing Flight Facility. Ten percent of the autolands terminated with a full stop, followed by a takeoff to set up for another approach. All of the approaches and landings were accomplished with the guidance coupled to the autopilot. Upon touchdown, the autopilot was disengaged, and the pilot assumed control of the aircraft. All test flights were flown in daytime visual meteorological conditions (VMC).

Overview of Flight Testing

A total of 111 approaches were conducted, with 110 resulting in successful autolands. When the aircraft was at about 300 ft of altitude on the 37th approach (following the bubble pass), the GPS Operational Control Segment temporarily turned off the signal of one of the GPS satellites for maintenance. This condition was detected at the airborne receiver's carrier tracking loop level. As intended in the design, the landing system responded by removing the ILS Tuned discrete signal, which disconnected the autopilot within 0.25 s of the initial event. The Category III specification for time-to-alarm due to a system fault is 2 s. The pilot then initiated a missed approach. The current nine-channel system would have allowed the landing to continue past such rare events using redundant GPS satellites. Out of the total of 111 approaches flown, the RAIM algorithm and other on-board safeguards issued no false alarms and resulted in no missed detections. For more information on the RAIM algorithm and how nominal protection limits are set at 0.5 m, see [10].

Navigation Sensor Error (NSE)

Figure 6 shows the vertical (most challenging dimension) NSE for 100 of the autolands using the laser tracker as a reference. The plot is given as a function of distance to the aim point, converted into units of altitude assuming the standard 3 deg flight path. To ensure that the approaches represent a true basis for operational evaluation, the plot shows only those 100 autolands for which the cycle ambiguities were intentionally reset (cleared) as a matter of procedure upon rollout onto final approach. (For experimentation purposes during some of the other autolands, it was demonstrated that the integers from a previous touch-and-go could be successfully carried around the pattern through to the next bubble pass.)

It is believed that the errors shown in Figure 6 are dominated by the laser tracker. The standard error signature of the angular-based laser tracker is readily apparent in the plot as the spread on the vertical error increases with range. Prior to the advent of GPS, laser trackers were traditionally considered the most accurate and convenient means of independently establishing position. It is interesting that GPS can be credited with finding new sources of error in laser trackers not previously considered or encountered in this application. In the flight trials at different test ranges, systematic errors found during data analysis on the order of tenths of a milliradian were traced to the omission of a correction for tropospheric refraction of the laser beam due to the gradient of atmospheric density with altitude.

As a demonstration of the capacity of IBLS to provide enhanced availability, most of the approaches shown used the satellite selection algorithm that picks the four highest-elevation satellites in the sky. Occasionally, this algorithm yields a PDOP greater than 10 for the four satellites. Interestingly, the positioning errors in these high-PDOP approaches are unnoticeable because they are

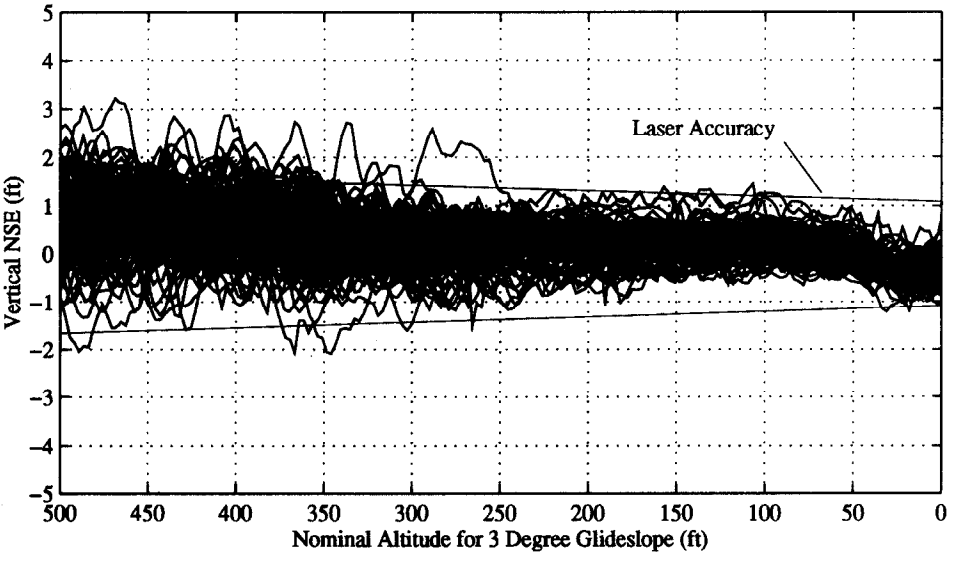

Fig. 6—Vertical Navigation Sensor Error (NSE) for 100 Autolands

still smaller than the laser errors. In Figure 6, even three autolands with satellite PDOP in the range of 17–18 do not stand out from the rest. In aircraft navigation applications with less-challenging performance requirements than Category III precision landing, a PDOP this large would be considered unusable with all other known GPS techniques. However, with IBLS, a satellite PDOP of 18 resulted in significantly less than 1 ft of vertical error and was employed for autolanding.

Figure 7 shows the NSEs in the cross-track direction. Again, the errors are believed to be dominated by the laser tracker.

Table 1 provides compiled ensemble statistics at 50 ft above runway threshold for all the approaches shown in the NSE plots. The landing system meets the requirements for NSE given in the ICAO Annex 10 document [1] and the U.S. Federal Radionavigation Plan (FRP) [11].

The navigation system performance can be evaluated in several ways. The raw position error, or NSE, was discussed earlier. The interaction of this error with the control system can be approximated by filtering the raw error using a control motion noise (CMN) filter and a path following error (PFE) filter. The output of the CMN filter is a measure of the unwanted control effort due to

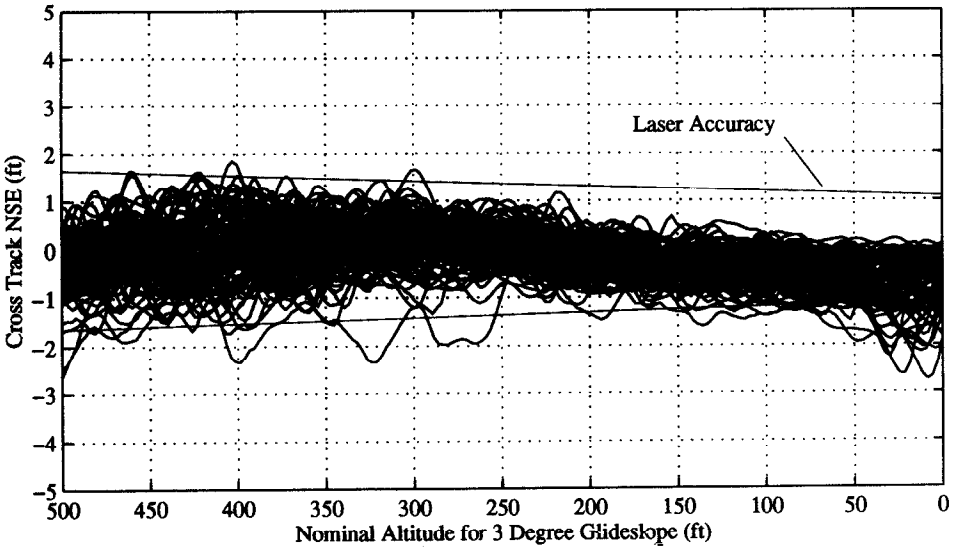

Fig. 7—Cross-Track Navigation Sensor Error (NSE) for 100 Autolands

Table 1—Navigation Sensor Error at 50 ft Above Threshold

NSE	Vertical (m)	Cross-Track (m)
Sigma (σ)	0.09	0.13
Mean (μ)	0.01	−0.19
$\lvert\mu\rvert + 2\sigma$ ($\approx$95%)	0.20	0.40
ICAO Annex 10	0.60	4.40
FRP	0.60	4.10
Meets Requirement	Yes	Yes

high-frequency components of the NSE. The output of the PFE filter is a measure of the aircraft position error resulting from the bias and low-frequency components of the NSE.

As mentioned before, the laser tracker errors are believed to be much larger than the IBLS errors. Therefore, the laser errors dominate the calculated NSE for these flight tests. However, the calculated NSE may be used to loosely bound the CMN and PFE performance of IBLS. Table 2 shows the 95 percent CMN and PFE at 50, 100, and 200 ft, and all altitudes less than 500 ft where centimeter-level positioning was initiated. The proposed 95 percent requirements [12] are also given. Although this table loosely bounds the IBLS performance, the proposed requirements are met.

Total System Error

Figure 8 shows the vertical total system error (TSE) for all 110 approaches as measured by the laser tracker. For comparison, the 95 percent required navigation performance (RNP) inner tunnel boundaries derived from [13] are superimposed on the plot. Given that the NSE for the approaches is less than 0.6 ft, it is believed that most of the TSE observed is due to the autopilot (flight technical error). The upward bend at the right of the plot results from the flare maneuver guided by the radar altimeter starting at 50 ft altitude.

Table 2—Vertical CMN and PFE for all 110 Approaches

Height (ft)	CMN (m)	PFE (m)
50	0.11	0.21
100	0.09	0.17
200	0.10	0.27
< 500	0.22	0.40
Proposed Requirements	0.70	1.80

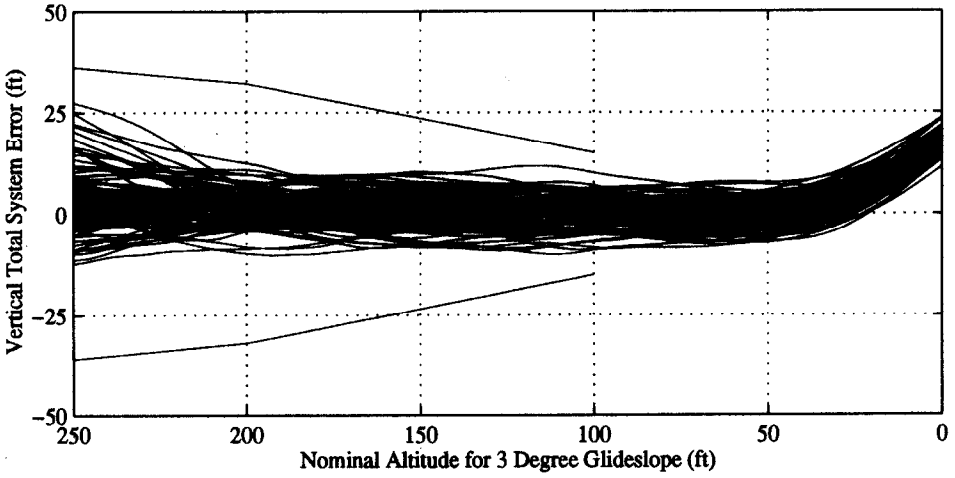

Fig. 8—Vertical Total System Error (TSE) Near Touchdown for 110 Autolands

Despite PDOPs as high as 18, circa 1985 quality code phase measurements from the GPS sensor, and crosswinds that on the third day of flight testing were on average 70 percent out of the 10 kn maximum specification of the autopilot, the performance is well within the RNP inner tunnel.

Figure 9 shows the lateral TSE. Again the error falls within the RNP inner tunnel requirements, despite crosswind components that significantly exceeded the autopilot specifications. Table 3 summarizes the TSE statistics for altitudes of 50 and 100 ft.

Although the TSE performance satisfied the RNP tunnel requirements, larger-than-desired transients at the bubble exit occurred in some cases during the testing. These transients had been expected when the decision was made to use the six-channel receiver rather than the new nine-channel system. The situation is analogous to a worst-case appearance of code multipath coupled simultaneously with a satellite outage that leaves poor satellite geometry and poor PDOP. Furthermore, on the third day of flight testing, the crosswinds were 70 percent out of the autopilot specification. With three worst-case conditions in effect *simultaneously*, the system remained well within the RNP tunnel to touchdown to satisfy Category III specifications.

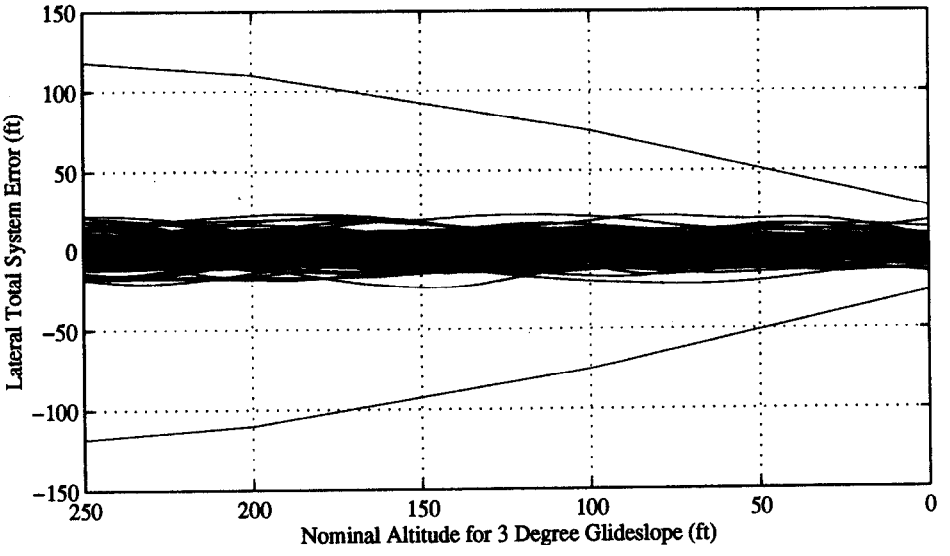

Fig. 9—Cross-Track Total System Error (TSE) for 110 Autolands

Table 3—Total System Error at 50 and 100 ft

TSE	Vertical 100 ft (m)	Lateral 100 ft (m)	Vertical 50 ft (m)	Lateral 50 ft (m)
Sigma (σ)	1.1	2.2	1.0	2.1
Mean (μ)	0.1	0.2	0.1	0.1
$\lvert\mu\rvert + 2\sigma$ ($\approx$95%)	2.3	4.6	2.1	4.3
RNP Inner Tunnel	4.6	22.9	(TBD)	15.5
Meets Requirement	Yes	Yes	Yes	Yes

Touchdown Dispersions

Figure 10 shows the touchdown dispersions for all 110 autolands. The weight-on-wheels signal was not available, so the touchdown times were approximated by looking at the height of the main landing gear as determined by IBLS. These times were confirmed by watching time-tagged videos of the landings. The ellipses in the figure represent the uncertainty in the touchdown points. A virtual ILS glide slope plane included the aim point. The actual touchdown points lie consistently after the aim point because of the flare maneuver. Superimposed on the figure is the nominal touchdown box. The positioning of the box is that given in AC-20-57A [3]. Despite high crosswinds, circa 1985 code phase noise, and high PDOPs, all 110 of the touchdown points are within this 95 percent touchdown box. Table 4 provides quantitative results.

SUMMARY AND OBSERVATIONS

The flight tests indicated that the system performance far exceeded Category III accuracy requirements. The accuracy of the GPS guidance and the straightforward integration into the 737 autopilot clearly demonstrated the feasibility of GPS and the Integrity Beacon Landing System (ILBS) for near-term Category III application on transport category aircraft. Hardware and software limitations of the test system caused some transients when the pseudolites were overflown, but these have already been eliminated in the current implementation.

IBLS was shown to be more than sufficient in meeting accuracy requirements for Category III automatic landings. But in addition to accuracy, architectural design and analysis are the primary means for establishing Category III integ-

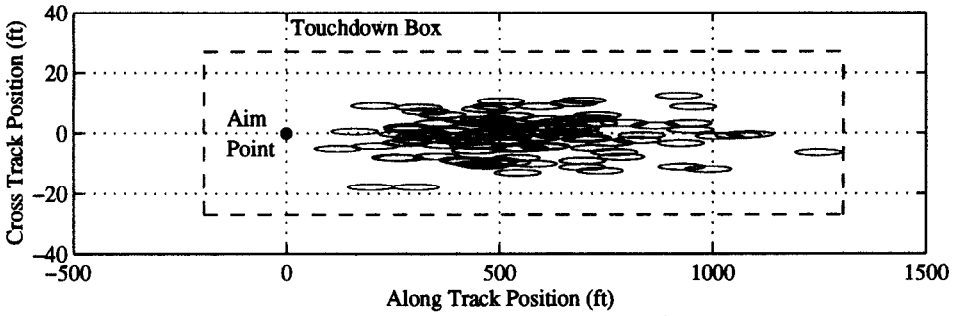

Fig. 10—Touchdown Dispersions for 110 Autolands

Table 4—Total System Touchdown Accuracy for 110 Autolands

Total System Accuracy (m)	Along-Track (m)	Cross-Track (m)
Sigma (σ)	66.5	1.9
Mean (μ)	1.9	0.4
$\lvert\mu\rvert + 2\sigma$ (95%)	134.9	4.2
AC-20-57A (95%)	228.5 (half-length)	8.2
Meets Requirement	Yes	Yes

rity. The integrity of the cycle ambiguity resolution process throughout the 111 approaches was 100 percent successful. No false alarms were issued, and no missed detections were registered.

CONCLUSIONS

The following conclusions can be drawn from the flight test results:

1) The vertical sensor accuracy of the Integrity Beacon Landing System (IBLS), including approaches with poor PDOP, provided a $|\mu| + 2\,\sigma$ of 0.6 ft ($\approx$95 percent) or better. Most of the error is believed to originate from the laser tracker.
2) IBLS meets the precision approach Category III vertical and cross-track accuracy requirements set forth in ICAO Annex 10.
3) During the flight testing, the landing system properly detected an actual anomaly within the GPS system.
4) The integrity of the system is being demonstrated through analysis and flight testing. With the centimeter-level precision and built-in receiver autonomous integrity monitoring (RAIM) of IBLS, it is believed that the probability of missed detection of failure is better than one in a billion.
5) The landings were carried out under challenging handicap conditions, which for some passes included simultaneous application of worst-case code phase noise, PDOP of 18, and out-of-specification crosswinds. In spite of these adverse conditions, all accuracy specifications were met.
6) The closed-loop characteristics of the system when connected to the autopilot exhibited performance well within the 95 percent touchdown box specification for Category III.
7) Category III precision landing using GPS on air transport aircraft appears technically feasible.

APPENDIX A
ABSOLUTE POSITIONING WITH INTEGRITY BEACONS

To provide further insight into how IBLS is able to provide such high performance accuracy and integrity using GPS, this appendix provides the matrix formulation of cycle ambiguity resolution. Figure 11 serves as a guide for the vector definitions employed herein. No loss of generality is incurred by assuming for this formulation that the aircraft receive antenna is a single point.

Single differencing of raw carrier phase measurements obtained at airborne and reference station receivers yields for SV i at epoch k:

$$\varphi_{ik} = -\hat{\mathbf{s}}_{ik}^{T}\mathbf{x}_k + \tau_k + N_i^s + \epsilon_{ik}^s \qquad \text{(A-1)}$$

where φ_{ik} is the single-differenced (aircraft minus reference) SV phase, $\hat{\mathbf{s}}_{ik}$ is the line-of-sight unit vector to the SV, $\mathbf{x}_k$ is the displacement vector from the differential station GPS receive antenna to the top-mounted aircraft GPS antenna, τ_k is the difference between the aircraft and reference receiver clock biases, N_i^s is the satellite integer cycle ambiguity, and ϵ_{jk}^s is the satellite range measurement error due to multipath and receiver noise. Similarly for Integrity Beacon j at epoch k:

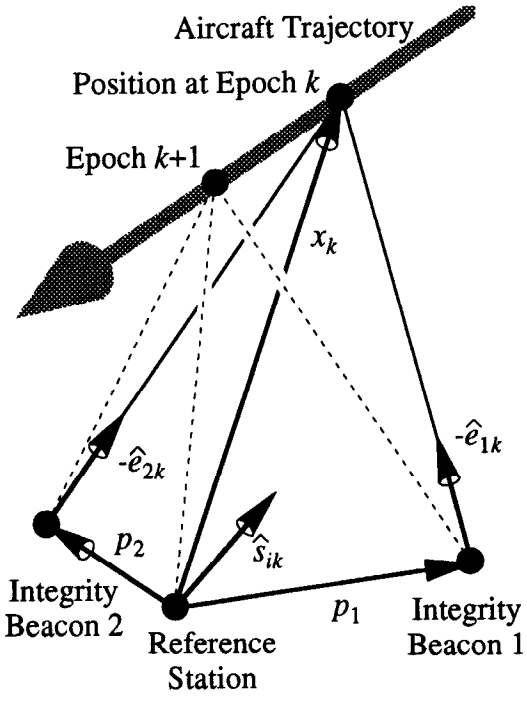

Fig. 11—Vector Geometry

$$\phi_{jk} = |\mathbf{p}_j - \mathbf{x}_k| - |\mathbf{p}_j| + \tau_k + N_j^p + \epsilon_{jk}^p, \tag{A-2}$$

where ϕ_{jk} is the single-differenced Integrity Beacon phase, and $\mathbf{p}_j$ is the vector from the differential station to Integrity Beacon j. Since the transmitter is quite close, the formulation for satellites (whose wave fronts are essentially planar) is not appropriate. Instead, the use of range magnitude is necessary.

Given an approximate trajectory $\bar{\mathbf{x}}_k$ obtained from code-based differential GPS, the equations above can be expressed in terms of the deviation from the approximate trajectory: $\delta\mathbf{x}_k \equiv \mathbf{x}_k - \bar{\mathbf{x}}_k$. Keeping first-order terms only, the result is

$$\begin{aligned} \delta\varphi_{ik} &\equiv \varphi_{ik} + \hat{\mathbf{s}}_{ik}^T\bar{\mathbf{x}}_k = -\hat{\mathbf{s}}_{ik}^T\delta\mathbf{x}_k + \tau_k N_i^s + \epsilon_{ik}^s \\ \delta\phi_{jk} &\equiv \phi_{jk} - |\mathbf{p}_j - \bar{\mathbf{x}}_k| + |\mathbf{p}_j| = -\hat{\mathbf{e}}_{jk}^T\delta\mathbf{x}_k + \tau_k + N_j^p + \epsilon_{jk}^p \end{aligned} \tag{A-3}$$

where $\hat{\mathbf{e}}_{jk}^T \equiv (\mathbf{p}_j - \bar{\mathbf{x}}_k)/|\mathbf{p}_j - \bar{\mathbf{x}}_k|$. To resolve cycle ambiguities, the value of one integer must be specified because of the existence of the clock bias τ_k, which is common to all measurements at epoch k. For simplicity, we choose $N_1^s = 0$. Defining $\delta\Phi_k$ to be the vector of m SV and two Integrity Beacon measurements at epoch k,

$$\delta\Phi_k \equiv \begin{bmatrix} \delta\varphi_{1k} \\ \vdots \\ \delta\phi_{mk} \\ \delta\phi_{1k} \\ \delta\phi_{2k} \end{bmatrix}, \text{ and } \hat{\mathbf{S}}_k \text{ as } \hat{\mathbf{S}}_k \equiv \begin{bmatrix} -\hat{\mathbf{s}}_{1k}^T & 1 \\ \vdots & \vdots \\ -\hat{\mathbf{s}}_{mk}^T & 1 \\ -\hat{\mathbf{e}}_{1k}^T & 1 \\ -\hat{\mathbf{e}}_{2k}^T & 1 \end{bmatrix} \tag{A-4}$$

we stack all n measurements collected during Integrity Beacon overpass to obtain

$$\begin{vmatrix} \delta\Phi_1 \\ \vdots \\ \delta\Phi_k \\ \vdots \\ \delta\Phi_n \end{vmatrix} = \begin{vmatrix} \hat{\mathbf{S}}_1 & 0 & \cdots & 0 & 0 & \bar{\mathbf{I}} \\ 0 & \ddots & 0 & \ddots & 0 & \vdots \\ \vdots & \ddots & \hat{\mathbf{S}}_k & \ddots & \vdots & \bar{\mathbf{I}} \\ 0 & \ddots & 0 & \ddots & 0 & \vdots \\ 0 & 0 & \cdots & 0 & \hat{\mathbf{S}}_n & \bar{\mathbf{I}} \end{vmatrix} \begin{vmatrix} \delta\mathbf{x}_1^* \\ \vdots \\ \delta\mathbf{x}_k^* \\ \vdots \\ \delta\mathbf{x}_n^* \\ \mathbf{N} \end{vmatrix} + \epsilon \tag{A-5}$$

where $\bar{\mathbf{I}} = \begin{bmatrix} 0 & \cdots & 0 \\ 1 & \cdots & 0 \\ \vdots & \ddots & \vdots \\ 0 & \cdots & 1 \end{bmatrix}$, $\delta\mathbf{x}_k^* = \begin{bmatrix} \delta\mathbf{x} \\ \tau_k \end{bmatrix}$, and $\mathbf{N} = [N_2^s \cdots N_m^s \; N_1^p \; N_2^p]^T$.

The least-squares solution to the above can be obtained efficiently by sparse matrix batch algorithms or equivalently by sequential forward-backward smoothing. Because of the nonlinear nature of the problem, the "solution" $\delta\mathbf{x}_k$ is not the final answer. Instead, the approximate trajectory and observation matrix must be improved by the computed estimate of $\delta\mathbf{x}_k$, and the process above repeated through convergence (i.e., until the update $\delta\mathbf{x}_k$ becomes negligible). Computation for convergence takes considerably less than 1 s on a 25 MHz 486 PC. Experience has shown that the solution converges in three to six iterations. The current algorithm was tested in simulation and always converged when presented with an initial condition within 300 m of the correct value for a 100 m altitude bubble pass. In repetitive flight trials presented in the paper, the algorithm converged on every approach. In the unlikely event of convergence failure, the alert to the pilot would be a continuity problem, *not* an integrity problem.

The final solution is an 'absolute' position fix in that it is given in the absolute desired runway coordinate frame.

APPENDIX B
POSITIONING AFTER THE BUBBLE PASS

At the end of the bubble pass, the trajectory is 'anchored' in the runway coordinate frame in an absolute sense so that any subsequent measurements of carrier phase can still be tied to the same coordinate frame. The derivation given here is abridged from that given in [14]. The carrier phase measurement equation can be written:

$$\boldsymbol{\phi} = [\mathbf{G}\ \mathbf{I}] \begin{pmatrix} \mathbf{x} \\ \tau \\ \mathbf{N} \end{pmatrix} + \delta\boldsymbol{\phi} \tag{B-1}$$

where $\boldsymbol{\phi}$ (n × 1) is the single-difference carrier phase measurement (expressed in L1 wavelengths), $\mathbf{G}$ (n × 4) is the traditional GPS geometry matrix, $\mathbf{I}$ (n × n) is the identity matrix, $\mathbf{x}$ (3 × 1) is the position, τ (scalar) is the differential receiver clock bias, $\mathbf{N}$ (n × 1) are the integers, $\delta\boldsymbol{\phi}$ (n × 1) are the measurement errors (including reference phase prediction errors), and n is the number of satellites.

If an integer estimate, $\hat{\mathbf{N}}$, and the corresponding covariance, $\mathbf{P}_N$, are available, this equation can be rewritten:

$$\boldsymbol{\phi} - \hat{\mathbf{N}} = \mathbf{G}\begin{pmatrix} \mathbf{x} \\ \tau \end{pmatrix} + (\tilde{\mathbf{N}} + \delta\boldsymbol{\phi}) \tag{B-2}$$

where $\tilde{\mathbf{N}}$ is the error in the integer estimate. Assuming the measurement errors are uncorrelated with variance σ^2, a weighted least-squares position/clock estimate can be calculated:

$$\begin{pmatrix} \hat{\mathbf{x}} \\ \hat{\tau} \end{pmatrix} = [\mathbf{G}^T\mathbf{R}_e^{-1}\mathbf{G}]^{-1}\,\mathbf{G}^T\mathbf{R}_e^{-1}(\boldsymbol{\phi} - \hat{\mathbf{N}}) \tag{B-3}$$

with covariance $\mathbf{P}_{x\tau} = [\mathbf{G}^T\mathbf{R}_e^{-1}\mathbf{G}]^{-1}$, where $\mathbf{R}_e \equiv \sigma^2\mathbf{I} + \mathbf{P}_N$.

RAIM is performed to verify that each new measurement is consistent with the existing integer estimates. If the measurement does not pass this check, the approach can be aborted. In some cases, the failure may be isolated. Isolation has not yet been implemented in the real-time software.

To perform RAIM using the carrier phase, the measurement equation is transformed into the following form, where the measurement is only a function of the integers:

$$\mathbf{z} = \mathbf{H}\mathbf{N} + \boldsymbol{\nu} \tag{B-4}$$

$$E[\boldsymbol{\nu}\boldsymbol{\nu}^T] = \mathbf{R} \tag{B-5}$$

This transformation is accomplished by premultiplying the carrier phase measurement equation by $\mathbf{L}$, where the rows of $\mathbf{L}$ make up an orthonormal basis for the left null space of $\mathbf{G}$:

$$\mathbf{L}\boldsymbol{\phi} = \mathbf{L}\mathbf{N} + \mathbf{L}\delta\boldsymbol{\phi}$$

$$\mathbf{z} = \mathbf{L}\boldsymbol{\phi}$$

$$\mathbf{H} = \mathbf{L}$$

$$\mathbf{R} = \sigma^2\mathbf{L}\mathbf{L}^T = \sigma^2\mathbf{I}$$

The position and clock terms have been eliminated from the measurement, leaving a reduced measurement that is a function of the integers alone. The difference between the expected and the actual reduced measurement is calculated:

$$\mathbf{r} \equiv E[\mathbf{z}] - \mathbf{z} = E[\mathbf{H}\mathbf{N} + \boldsymbol{\nu}] - \mathbf{H}\mathbf{N} - \boldsymbol{\nu}$$

$$\mathbf{r} = \mathbf{H}(\hat{\mathbf{N}} - \mathbf{N}) - \boldsymbol{\nu} = \mathbf{H}\tilde{\mathbf{N}} - \boldsymbol{\nu} \tag{B-6}$$

This residual quantity, **r**, is a random vector with zero mean and covariance given by:

$$\mathbf{P}_r = \mathbf{H}\mathbf{P}_N\mathbf{H}^T + \mathbf{R}$$

A measure of the consistency of the new measurement is the weighted residual:

$$\mathbf{w} = \mathbf{r}^T\mathbf{P}_r^{-1}\mathbf{r}$$

If this weighted residual is greater than some predetermined threshold, a RAIM alert is issued. The threshold is a function of the dimension of **r** and the desired continuity. Just as in [10], integrity can be taken as the dependent variable.

ACKNOWLEDGMENTS

The authors wish to express their gratitude to a number of individuals and organizations who helped carry out these flight tests. At Stanford, Andy Barrows, Mike O'Connor, Konstantin Gromov, Gabe Elkaim, Jock Christie, Dr. Hiro Uematsu, Chris Shaw, and many others provided enormous assistance. The Marrings and the Dompe family of Central Valley, California are gratefully acknowledged for allowing the use of their property beneath the approach path of Runway 35 to conduct these experiments. Elsinore Aerospace, including Jeff Dolph and Mark Ostendorf, and United's maintenance staff at SFO did an excellent job of planning, installing, and de-installing this experiment with complete success in rapid time. Trimble Navigation, Ltd. is acknowledged for its cooperation in providing GPS equipment. Sponsorship for the flight tests was provided by the Satellite Program Office of the Federal Aviation Administration.

REFERENCES

1. *International Standards, Recommended Practices and Procedures for Air Navigation Services—Annex 10*, ICAO, April 1985.
2. McFarland, R. H. and Quinet, D., *Selection of a Localizer Array for Use When Large Buildings Are Present*, The Institute of Navigation National Technical Meeting, San Diego, CA, January 1994, p. 219.
3. Federal Aviation Administration, *Automatic Land Sustem (ALS)*, Advisory Circular 20-57A, January 12, 1971.
4. Cohen, C. E., Pervan, B., Cobb, H. S., Lawrence, D., Powell, J. D., and Parkinson, B. W., *Real-Time Cycle Ambiguity Resolution Using a Pseudolite for Precision Landing of Aircraft with GPS*, DSNS-93, Amsterdam, The Netherlands, March–April 1993.
5. Cohen, C. E., Pervan, B., Cobb, H. S., Lawrence, D., Powell, J. D., and Parkinson, B. W., *Real-Time Flight Test Evaluation of the* GPS Marker Beacon *Concept for Category III Kinematic GPS Precision Landing*, ION GPS-93, Salt Lake City, UT, September 1993.
6. Cohen, C. E., Pervan, B., Cobb, H. S., Lawrence, D., Powell, J. D., and Parkinson, B. W., *Achieving Required Navigation Performance Using GNSS for Category III Precision Landing*, DSNS-94, London, UK, April 1994.
7. Cohen, C. E., Lawrence, D. G., Pervan, B. S., Cobb, H. S., Barrows, A. K., Powell, J. D., Parkinson, B. W., Wullschleger, V., and Kalinowski, S., *Flight Test Results of Autocoupled Approaches Using GPS and Integrity Beacons*, ION GPS-94, Salt Lake City, UT, September 20–24, 1994.

8. Pervan, B. S., Cohen, C. E., and Parkinson, B. W., *Integrity Monitoring for Precision Approach Using Kinematic GPS and a Ground-Based Pseudolite*, NAVIGATION, Journal of The Institute of Navigation, Vol. 41, No. 2, Summer 1994.
9. Pervan, B. S., Cohen, C. E., and Parkinson, B. W., *Integrity in Cycle Ambiguity Resolution for GPS-Based Precision Landing*, DSNS '94, London, United Kingdom, April 18–22, 1994.
10. Pervan, B. S., Cohen, C. E., Lawrence, D. G., Cobb, H. S., Powell, J. D., and Parkinson, B. W., *Autonomous Integrity Monitoring for GPS-Based Precision Landing Using Integrity Beacon Pseudolites*, ION GPS-94, Salt Lake City, UT, September 1994.
11. *U.S. Federal Radionavigation Plan,* Departments of Transportation and Defense, 1992.
12. *FAA Operational Requirements Document, Local Area Augmentation System (LAAS),* February 1995.
13. Kelly, R. J. and Davis, J. M., *Required Navigation Performance (RNP) for Precision Approach and Landing with GNSS Application*, NAVIGATION, Journal of The Institute of Navigation, Vol. 41, No. 1, Spring 1994.
14. Lawrence, D., Pervan, B., Cohen, C., Cobb, H. S., Powell, J. D., and Parkinson, B. W., *A Real-Time Architecture for Kinematic GPS Applied to the Integrity Beacon Landing System*, 51st Annual Meeting of The Institute of Navigation, Colorado Springs, CO, June, 1995.